

# BCS-BEC crossovers and unconventional phases in dilute nuclear matter

Martin Stein\* and Armen Sedrakian†

*Institute for Theoretical Physics, J. W. Goethe-University,  
D-60438 Frankfurt am Main, Germany*

Xu-Guang Huang‡

*Physics Department & Center for Particle Physics and Field Theory,  
Fudan University, Shanghai 200433, China*

John W. Clark§

*Department of Physics and McDonnell Center for the Space Sciences,  
Washington University, St. Louis, Missouri 63130, USA and  
Centro de Ciências Matemáticas, University of Madeira, 9000-390 Funchal, Portugal*

(Dated: July 31, 2018)

We study the phase diagram of isospin-asymmetrical nuclear matter in the density-temperature plane, allowing for four competing phases of nuclear matter: (i) the unpaired phase, (ii) the translationally and rotationally symmetric, but isospin-asymmetrical BCS condensate, (iii) the current-carrying Larkin-Ovchinnikov-Fulde-Ferrell phase, and (iv) the heterogeneous phase-separated phase. The phase diagram of nuclear matter composed of these phases features two tri-critical points in general, as well as crossovers from the asymmetrical BCS phase to a BEC of deuterons plus a neutron gas, both for the homogeneous superfluid phase (at high temperatures) and for the heterogeneous phase (at low temperatures). The BCS-BEC type crossover in the condensate occurs as the density is reduced. We analyze in detail some intrinsic properties of these phases, including the Cooper-pair wave function, the coherence length, the occupation numbers of majority and minority nucleonic components, and the dispersion relations of quasiparticle excitations about the ground state. We show by explicit examples that the physics of the individual phases and the transition from weak to strong coupling can be well understood by tracing the behavior of these quantities.

PACS numbers: 21.65.+f, 21.30.Fe, 26.60.+c

## I. INTRODUCTION

The two-nucleon vacuum interactions at low energies are well constrained by the phase-shift data derived from the analysis of elastic nucleon-nucleon collisions. Therefore, the main theoretical challenge of understanding nuclear matter at sub-saturation densities stems from the complexity of the many-body physics. The attractive part of the nuclear interaction is responsible for the formation of nuclear clusters, as well as condensates of Bardeen-Cooper-Schrieffer (BCS) type at low temperatures. The temperature, density, and isospin asymmetry of such matter are relevant for the description of supernovae and neutron stars. These two astrophysical venues differ somewhat in the respective ranges of these variables. For example, in supernovae the isospin asymmetries are much smaller than in cold  $\beta$ -catalyzed neutron-star matter. Consequently in neutron-star matter  $^1S_0$  pairing in the isospin-triplet, spin-singlet state of neutrons is favored, whereas nearly isospin-symmetrical matter supports  $^3S_1$ - $^3D_1$  pairing in the spin-triplet, isospin-

singlet state.

Fermionic BCS superfluids, which form loosely bound Cooper pairs at weak coupling, undergo a transition to the Bose-Einstein condensate (BEC) state of tightly bound bosonic dimers, once the pairing strength increases sufficiently [1, 2]. This behavior has been confirmed in experiments on cold atomic gases, where the interactions can be manipulated via the Feshbach mechanism. In isospin-symmetric nuclear matter, the transition from the BCS to the BEC state of the  $^3S_1$ - $^3D_1$  condensate may occur upon dilution of the system, in which case the asymptotic state is a Bose-Einstein condensate of deuterons [3–16]. Isospin asymmetry, induced by weak interactions in stellar environments and expected in exotic nuclei, disrupts isoscalar neutron-proton ( $np$ ) pairing, because the mismatch in the Fermi surfaces of protons and neutrons suppresses the pairing correlations [17]. The standard Nozières-Schmitt-Rink theory [1] of the BCS-BEC crossover must also be modified, such that the low-density asymptotic state becomes a gaseous mixture of neutrons and deuterons [18]. The  $^3S_1$ - $^3D_1$  condensates can be important in a number of physical settings. (i) Low-energy heavy-ion collisions produce large amounts of deuterons in final states as putative fingerprints of  $^3S_1$ - $^3D_1$  condensation [4]. (ii) Large nuclei may feature spin-aligned  $np$  pairs, as evidenced by recent experimental findings [19] on excited states in  $^{92}\text{Pd}$ ; moreover, exotic nuclei with extended halos provide a lo-

\*Electronic address: mstein@th.physik.uni-frankfurt.de

†Electronic address: sedrakian@th.physik.uni-frankfurt.de

‡Electronic address: huangxuguang@fudan.edu.cn

§Electronic address: jwc@wuphys.wustl.edu

cus for  $n$ - $p$  Cooper pairing. (iii) Directly relevant to the parameter ranges covered in the present study are the observations that supernova and hot proto-neutron-star matter at sub-saturation densities have low temperature and low isospin asymmetry, and that the deuteron fluid is a substantial constituent [20, 21].

Two relevant energy scales for the problem domain under study are provided by the magnitude of the shifts  $\pm\delta\mu = \pm(\mu_n - \mu_p)/2$  of the chemical potentials  $\mu_n$  and  $\mu_p$  of neutrons and protons from their common value  $\bar{\mu}$ , and the pairing gap  $\Delta_0$  in the  ${}^3S_1$ - ${}^3D_1$  channel at  $\delta\mu = 0$ . With increasing isospin asymmetry, i.e., as  $\delta\mu$  increases from zero to values of order  $\Delta_0$ , a sequence of unconventional phases may emerge. One of these is a neutron-proton condensate whose Cooper pairs have nonzero center-of-mass (c. m.) momentum [8, 22, 23]; this phase is the analog of the Larkin-Ovchinnikov-Fulde-Ferrell (LOFF) phase in electronic superconductors [24, 25]. Another possibility is phase separation (PS) into superconducting and normal components, proposed in the context of cold atomic gases [26]. An alternative to the LOFF phase is the deformed Fermi surface (DFS) phase, which, unlike the LOFF phase, is translationally invariant but breaks the rotational symmetry [23, 27]. Because these two phases share many common properties, we shall concentrate only on the LOFF phase. At large isospin asymmetry, where  ${}^3S_1$ - ${}^3D_1$  pairing is strongly suppressed, a BCS-BEC crossover may also occur in the isotriplet  ${}^1S_0$  pairing channel, notably in neutron-rich systems and halo nuclei [28–35]. As inferred from the experimental phase shifts, the pairing force in the  ${}^3S_1$ - ${}^3D_1$  channel is stronger than in the  ${}^1S_0$  channel. Isotriplet-spin-triplet pairing is prohibited by the Pauli principle; accordingly, isotriplet pairing occurs only in the spin-singlet channel. Because isosinglet-spin-triplet pairing is favored over isotriplet spin-singlet pairing for not very high asymmetries, we neglect isotriplet pairing. For large asymmetries, isosinglet pairing is strongly suppressed and pairing takes place mostly in the isotriplet spin-singlet channel. Simple  ${}^1S_0$  pairing only occurs for chemical potentials in the continuum of two-particle scattering states. However, pairing in the  ${}^3S_1$ - ${}^3D_1$  channel can arise for values of the chemical potentials below the continuum edge, which is the case that corresponds to bound states (deuterons).

In the first paper (I) of this series [36], the concepts of unconventional  ${}^3S_1$ - ${}^3D_1$  pairing and the BCS-BEC crossover were unified in a model of isospin-asymmetrical nuclear matter by including some of the phases mentioned above. A phase diagram for superfluid nuclear matter was constructed over wide ranges of density, temperature, and isospin asymmetry. The coupled equations for the gap and the densities of the constituents (neutrons and protons) were solved allowing for the ordinary BCS state, its low-density asymptotic counterpart BEC state, and two phases that owe their existence to the isospin asymmetry: the phase with a current-carrying condensate (LOFF phase) and the phase in which the normal

fluid and superfluid occupy separate spatial domains. The latter phase is referred to as the phase-separated BCS (PS-BCS) phase and, in the strong-coupling regime, the phase-separated BEC (PS-BEC) phase. In this phase the asymmetry is accumulated in the normal domains, whereas the superfluid domain is perfectly isospin symmetric.

While the basic parameters of the superfluid phases, such as the pairing gap and energy density have been studied extensively across the BCS-BEC crossover, as well as in unconventional phases such as the LOFF phase, some *intrinsic features* characterizing the condensate are less well known. These include the Cooper-pair wave function, the occupation probabilities of particles, the coherence length, and related quantities. However, an understanding of the evolution of these properties during the transitions from BCS to unconventional (LOFF) phases as well as from weak to strong coupling provide important insights into the mechanisms underlying the emergence of new phases as well as into their nature. The present paper reports results from a study of these aspects of the pairing problem for the example of the  ${}^3S_1$ - ${}^3D_1$  condensate carried out within the framework developed in our previous work [36]. The LOFF phase is chosen as a representative of the unconventional phases. If PS takes place, one of the phases involved is the isospin-symmetrical BCS phase, whereas the other is the normal isospin-asymmetrical phase. Therefore, the intrinsic features of the superfluid component of this phase, as specified above, are identical to those of the BCS phase. Hence we do not discuss the intrinsic properties of the PS-BCS phase.

To induce a BCS-BEC crossover in the condensate properties, we use as a control parameter the adjustable density of the system. The relevant energies for scattering of two nucleons in the medium are set essentially by their Fermi energies and in turn by the density of the medium; hence the nuclear interaction strengths change with density as well.

Accordingly, the BCS-BEC crossover is enforced by two effects: a progressive dilution of the system and a concomitant increase in the interaction strength in the  ${}^3S_1$ - ${}^3D_1$ -channel at the lower energies involved. In the present study, we additionally vary the isospin asymmetry to generate a mismatch in the Fermi surfaces of paired fermions, and we change the temperature to access the entire density-temperature-asymmetry plane. It is worthwhile to note that in ultracold atomic gases the BCS-BEC crossover is achieved in a controlled manner by changing the effective interaction strengths via the Feshbach mechanism, whereas the mismatch of Fermi surfaces is achieved by trapping different amounts of atoms in a different hyperfine states.

This paper is structured as follows. In Sec. II we give a brief discussion of the theory of asymmetrical nuclear matter in the language of imaginary-time finite-temperature Green's functions. In Sec. III we discuss the phase diagram of asymmetrical nuclear matter

(Sec. III A), the temperature/asymmetry behavior of the gap in the weak-coupling regime (Sec. III B), the kernel of the gap equation in BCS and LOFF phases in various coupling regimes (Sec. III C), the Cooper-pair wave function across the BCS-BEC crossover (Sec. III D), and occupation numbers and quasiparticle dispersion relations (Sec. III E and III F, respectively). Our conclusions are summarized in Sec. IV.

## II. THEORY

The Green's function of the superfluid, written in the Nambu-Gor'kov basis, is given by

$$i\mathcal{G}_{12} = i \begin{pmatrix} G_{12}^+ & F_{12}^- \\ F_{12}^+ & G_{12}^- \end{pmatrix} = \begin{pmatrix} \langle T_\tau \psi_1 \psi_2^+ \rangle & \langle T_\tau \psi_1 \psi_2 \rangle \\ \langle T_\tau \psi_1^+ \psi_2^+ \rangle & \langle T_\tau \psi_1^+ \psi_2 \rangle \end{pmatrix}, \quad (1)$$

where  $G_{12}^+ \equiv G_{\alpha\beta}^+(x_1, x_2)$ , etc.,  $x = (t, \mathbf{r})$  denotes the continuous temporal-spatial variable, and Greek indices label discrete spin and isospin variables. Each operator in Eq. (1) can be viewed as a bi-spinor, i.e.,  $\psi_\alpha = (\psi_{n\uparrow}, \psi_{n\downarrow}, \psi_{p\uparrow}, \psi_{p\downarrow})^T$ , where the internal variables  $\uparrow, \downarrow$  label a particle's spin and the indices  $n, p$  label its isospin.

The matrix propagator (1) obeys the familiar Dyson equation

$$(\mathcal{G}_{0,13}^{-1} - \Xi_{13}) \mathcal{G}_{32} = \delta_{12}, \quad (2)$$

where  $\Xi_{12}$  is the matrix self-energy and the summation and integration over repeated indices are implicit. Equation (2) can be transformed into momentum space, where it becomes an algebraic equation. For our purposes, translational invariance cannot be assumed, so we proceed by defining relative  $\tilde{r} = x_1 - x_2$  and c. m.  $R = (x_1 + x_2)/2$  coordinates and Fourier transforming with respect to the relative four-coordinate and c. m. three-coordinate  $\mathbf{R}$ . The associated relative momentum is denoted below by  $k \equiv (ik_\nu, \mathbf{k})$  and the three-momentum of the c. m. is denoted by  $\mathbf{Q}$ . The zero component of the vector  $k$  takes on discrete values  $k_\nu = (2\nu + 1)\pi T$ , where  $\nu \in \mathbb{Z}$  and  $T$  is the temperature.

The relevant Fourier transformations can be obtained by first performing a variable transformation to the c. m. and relative coordinates

$$iG_{12}^+ = iG_{\tau\sigma, \tau'\sigma'}^+(\mathbf{x}_1, \mathbf{x}_2, \tilde{t}) = \left\langle T \psi_{\tau\sigma} \left( \mathbf{R} + \frac{\tilde{r}}{2}, 0 \right) \psi_{\tau'\sigma'}^+ \left( \mathbf{R} - \frac{\tilde{r}}{2}, \tilde{t} \right) \right\rangle, \quad (3)$$

where to exploit the time translation invariance we have defined the relative time variable  $\tilde{t} = t' - t$ . The Fourier transformations from the space-time to the momentum-frequency domain are defined via

$$G_{\tau\sigma, \tau'\sigma'}^+(\mathbf{k}, \mathbf{Q}, \tilde{t}) = \frac{1}{(2\pi)^3} \int d^3\mathbf{R} d^3\tilde{\mathbf{r}} e^{-i(\tilde{\mathbf{r}} \cdot \mathbf{k} + \mathbf{R} \cdot \mathbf{Q})} G_{\tau\sigma, \tau'\sigma'}^+(\mathbf{x}_1, \mathbf{x}_2, \tilde{t}). \quad (4)$$

The Fourier transformation from the imaginary-time domain to the frequency domain is given by

$$G_{\tau\sigma, \tau'\sigma'}^+(\mathbf{k}, \mathbf{Q}, t) = \frac{1}{\beta} \sum_\nu e^{-ik_\nu t} G_{\tau\sigma, \tau'\sigma'}^+(ik_\nu, \mathbf{k}, \mathbf{Q}). \quad (5)$$

The Fourier transformations for the remaining elements of the matrix Green's function  $i\mathcal{G}_{12}$  are constructed in an analogous manner. With the definitions above, we obtain the Fourier image of Eq. (2) as

$$[\mathcal{G}_0(k, \mathbf{Q})^{-1} - \Xi(k, \mathbf{Q})] \mathcal{G}(k, \mathbf{Q}) = \mathbf{1}_{8 \times 8}. \quad (6)$$

Further reductions are possible owing to the fact that the normal propagators for the particles and holes are diagonal in the spin-isospin spaces, i.e.,  $(G^+, G^-) \propto \delta_{\alpha\alpha'}$ , i.e., the off-diagonal elements of  $\mathcal{G}_0^{-1}$  are zero. Writing out the non-vanishing components in the Nambu-Gorkov space explicitly, we obtain  $[\mathcal{G}_0(ik_\nu, \mathbf{k}, \mathbf{Q})^{-1}]_{11} =$

$-[\mathcal{G}_0(-ik_\nu, \mathbf{k}, -\mathbf{Q})^{-1}]_{22} = G_0^{-1}(ik_\nu, \mathbf{k}, \mathbf{Q})$ , where

$$G_0(k, \mathbf{Q})^{-1} = \text{diag}(ik_\nu - \epsilon_{n\uparrow}^+, ik_\nu - \epsilon_{n\downarrow}^+, ik_\nu - \epsilon_{p\uparrow}^+, ik_\nu - \epsilon_{p\downarrow}^+) \quad (7)$$

with

$$\epsilon_{n/p, \uparrow/\downarrow}^\pm = \frac{1}{2m^*} \left( \mathbf{k} \pm \frac{\mathbf{Q}}{2} \right)^2 - \mu_{n/p}, \quad (8)$$

which it is useful to separate into symmetrical anti-symmetrical parts with respect to the time-reversal operation by writing

$$\epsilon_{n\uparrow/\downarrow}^\pm = E_S - \delta\mu \pm E_A, \quad (9)$$

$$\epsilon_{p\uparrow/\downarrow}^\pm = E_S + \delta\mu \pm E_A, \quad (10)$$

where

$$E_S = \frac{Q^2/4 + k^2}{2m^*} - \bar{\mu}, \quad (11)$$

$$E_A = \frac{\mathbf{k} \cdot \mathbf{Q}}{2m^*}, \quad (12)$$

are the symmetrical and anti-symmetrical parts of the quasiparticle spectrum and  $\bar{\mu} \equiv (\mu_n + \mu_p)/2$ . The effective mass  $m^*$  is defined in the usual fashion in terms of the normal self-energy, bare mass  $m$ , and Fermi momentum  $p_F$ , specifically

$$m/m^* = 1 - (m/p)\partial_p \Xi_{11}|_{p=p_F}, \quad (13)$$

if we neglect the small mismatch between neutron and proton effective masses.

Keeping this mismatch implies the changes  $E_{S/A} \rightarrow E_{S/A}(1 \pm \delta_m)$  and  $\delta\mu \rightarrow \delta\mu + \mu\delta_m$ , where  $\delta_m = (m_n^* - m_p^*)/(m_n^* + m_p^*) \ll 1$ . In the analysis below,  $\delta_m$  lies in the range  $0 \leq |\delta_m| \leq 0.06$ , the upper bound being attained for the largest asymmetries and densities relevant to this study. The quasiparticle spectra in Eq. (7) are written in a general reference frame moving with the c. m. momentum  $\mathbf{Q}$  relative to a laboratory frame at rest. The spectrum of quasiparticles is seen to be two-fold degenerate; i.e., the SU(4) Wigner symmetry of the unpaired state

is broken down to spin SU(2). In fact this Wigner symmetry is always approximate, because the phase shifts in the isoscalar and isotriplet  $S$  waves differ, such that isosinglet pairing is stronger than isotriplet pairing in bulk nuclear matter.

The nucleon-nucleon scattering data indicates that the dominant attractive interaction in low-density nuclear matter is the  ${}^3S_1$ - ${}^3D_1$  partial wave, which leads to isoscalar (neutron-proton) spin-triplet pairing. Accordingly, the anomalous propagators have the property  $(F_{12}^+, F_{12}^-) \propto (-i\tau_y) \otimes \sigma_x$ , where  $\sigma_i$  and  $\tau_i$  are Pauli matrices in spin and isospin spaces. This implies that in the quasiparticle approximation, the self-energy  $\Xi$  has only off-diagonal elements in the Nambu-Gorkov space. Specifically,  $\Xi_{12} = \Xi_{21}^+ = i\Delta_{\alpha\beta}$ , with  $\Delta_{14} = \Delta_{23} = -\Delta_{32} = -\Delta_{41} \equiv \Delta$ , where  $\Delta$  is the (scalar) pairing gap in the  ${}^3S_1$ - ${}^3D_1$  channel. Thus the first multiplier on the left-hand-side of Eq. (6) is given by

$$\mathcal{G}_0^{-1} - \Xi = \begin{pmatrix} ik_\nu - \epsilon_{n\uparrow}^+ & 0 & 0 & 0 & 0 & 0 & 0 & i\Delta \\ 0 & ik_\nu - \epsilon_{n\downarrow}^+ & 0 & 0 & 0 & 0 & i\Delta & 0 \\ 0 & 0 & ik_\nu - \epsilon_{p\uparrow}^+ & 0 & 0 & -i\Delta & 0 & 0 \\ 0 & 0 & 0 & ik_\nu - \epsilon_{p\downarrow}^+ & -i\Delta & 0 & 0 & 0 \\ 0 & 0 & 0 & i\Delta & ik_\nu + \epsilon_{n\uparrow}^- & 0 & 0 & 0 \\ 0 & 0 & i\Delta & 0 & 0 & ik_\nu + \epsilon_{n\downarrow}^- & 0 & 0 \\ 0 & -i\Delta & 0 & 0 & 0 & 0 & ik_\nu + \epsilon_{p\uparrow}^- & 0 \\ -i\Delta & 0 & 0 & 0 & 0 & 0 & 0 & ik_\nu + \epsilon_{p\downarrow}^- \end{pmatrix}. \quad (14)$$

It is sufficient to consider only a  $4 \times 4$  block of the full  $8 \times 8$  matrix Dyson equation, as the remaining blocks do not contain new information. We consider then

$$\begin{pmatrix} ik_\nu - \epsilon_n^+ & 0 & 0 & i\Delta \\ 0 & ik_\nu - \epsilon_p^+ & -i\Delta & 0 \\ 0 & i\Delta & ik_\nu + \epsilon_n^- & 0 \\ -i\Delta & 0 & 0 & ik_\nu + \epsilon_p^- \end{pmatrix} \cdot \begin{pmatrix} G_n^+ & 0 & 0 & F_{np}^- \\ 0 & G_p^+ & F_{pn}^- & 0 \\ 0 & F_{np}^+ & G_n^- & 0 \\ F_{pn}^+ & 0 & 0 & G_p^- \end{pmatrix} = \text{diag}(1, 1, 1, 1). \quad (15)$$

The solutions of this equation provide the normal and anomalous Green's functions

$$G_{n/p}^\pm = \frac{ik_\nu \pm \epsilon_{p/n}^\mp}{(ik_\nu - E_{\mp/\pm}^+)(ik_\nu + E_{\pm/\mp}^-)}, \quad (16)$$

$$F_{np}^\pm = \frac{-i\Delta}{(ik_\nu - E_\pm^+)(ik_\nu + E_\mp^-)}, \quad (17)$$

$$F_{pn}^\pm = \frac{i\Delta}{(ik_\nu - E_\mp^+)(ik_\nu + E_\pm^-)}, \quad (18)$$

where the four branches of the quasiparticle spectrum are given by

$$E_r^a = \sqrt{E_S^2 + \Delta^2} + r\delta\mu + aE_A, \quad (19)$$

in which  $a, r \in \{+, -\}$ . When  $r = a$  and  $E_A > 0$  the shifts owing to the isospin asymmetry  $\delta\mu$  and owing to the c. m. momentum  $\mathbf{Q}$  add up; consequently the branches  $E_-^-$  and  $E_+^+$  are located farther away from the isospin-symmetrical spectrum than the branches with  $r \neq a$  for which these two factors compensate for each other. In mean-field approximation, the anomalous self-energy (pairing-gap) is determined by

$$\Delta(\mathbf{k}, \mathbf{Q}) = \frac{1}{4\beta} \int \frac{d^3 k'}{(2\pi)^3} \sum_\nu V(\mathbf{k}, \mathbf{k}') \text{Im} \left[ F_{np}^+(k'_\nu, \mathbf{k}', \mathbf{Q}) + F_{np}^-(k'_\nu, \mathbf{k}', \mathbf{Q}) - F_{pn}^+(k'_\nu, \mathbf{k}', \mathbf{Q}) - F_{pn}^-(k'_\nu, \mathbf{k}', \mathbf{Q}) \right], \quad (20)$$

where  $V(\mathbf{k}, \mathbf{k}')$  is the neutron-proton interaction potential.

We perform a partial-wave expansion in Eq. (20) and compute the Matsubara sum, which yields

$$\Delta_l(Q) = \frac{1}{4} \sum_{a,r,l'} \int \frac{d^3 k'}{(2\pi)^3} V_{l,l'}(k, k') \times \frac{\Delta_{l'}(k', Q)}{2\sqrt{E_S^2(k') + \Delta^2(k', Q)}} [1 - 2f(E_a^r)], \quad (21)$$

where  $V_{l,l'}(k, k')$  is the interaction in the  ${}^3S_1$ - ${}^3D_1$  partial wave,  $f(\omega) = 1/[\exp(\omega/T) + 1]$ , and  $\Delta^2 = \sum_l \Delta_l^2$ .

The densities of neutrons and protons in any of the superfluid states are obtained by observing that

$$\begin{aligned} \rho_{n/p}(Q) &= \frac{2}{\beta} \int \frac{d^3 k}{(2\pi)^3} \sum_{\nu} G_{n/p}^+(k_{\nu}, \mathbf{k}, Q) \\ &= 2 \int \frac{d^3 k}{(2\pi)^3} \left[ \frac{1}{2} \left( 1 + \frac{E_S}{\sqrt{E_S^2 + \Delta^2}} \right) f(E_{\mp}^+) \right. \\ &\quad \left. + \frac{1}{2} \left( 1 - \frac{E_S}{\sqrt{E_S^2 + \Delta^2}} \right) f(-E_{\pm}^-) \right]. \quad (22) \end{aligned}$$

The magnitude  $Q$  of the c. m. momentum in Eqs. (22) and (21) is a parameter to be determined by minimizing the free energy of the system. For the homogeneous (but possibly translationally noninvariant) cases it suffices to find the minimum of the free energy of the superfluid (S) or unpaired (N) phase,

$$F_S = E_S - TS_S, \quad F_N = E_N - TS_N, \quad (23)$$

where  $E$  is the internal energy (statistical average of the system Hamiltonian) and  $S$  denotes the entropy. The free energy of the heterogeneous superfluid phase, which corresponds to separation of the normal and superfluid phases, is constructed as a linear combination,

$$\mathcal{F}(x, \alpha) = (1-x)F_S(\alpha=0) + xF_N(\alpha \neq 0), \quad (Q=0), \quad (24)$$

where  $x$  here denotes the filling fraction of the unpaired component and

$$\alpha = \frac{\rho_n - \rho_p}{\rho_n + \rho_p} \quad (25)$$

is the density asymmetry. In the superfluid phase (S) one has  $\rho_n^{(S)} = \rho_p^{(S)} = \rho^{(S)}/2$ , while in the unpaired phase (N) the neutron and proton partial densities are rescaled to new values  $\rho_{n/p}^{(N)}$ . Thus, the net densities of neutrons/protons per unit volume are given by  $\rho_{n/p} = (1/2)(1-x)\rho^{(S)} + x\rho_{n/p}^{(N)}$ .

The four possible states we consider are characterized as follows:

$$\begin{cases} Q = 0, \Delta \neq 0, x = 0, & \text{BCS phase,} \\ Q \neq 0, \Delta \neq 0, x = 0, & \text{LOFF phase,} \\ Q = 0, \Delta \neq 0, x \neq 0, & \text{PS phase,} \\ Q = 0, \Delta = 0, x = 1, & \text{unpaired phase,} \end{cases} \quad (26)$$

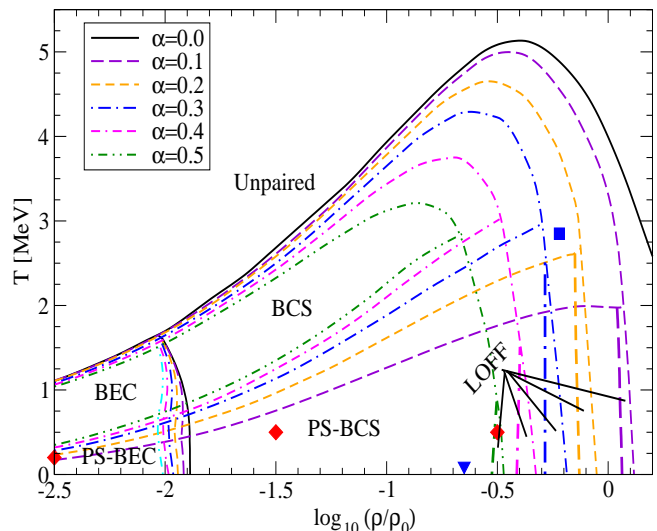


FIG. 1: (Color online) Phase diagram of dilute nuclear matter in the temperature-density plane for several isospin asymmetries  $\alpha$  (see also Ref. [36]). Here  $\rho_0 = 0.16 \text{ fm}^{-3}$  is the nuclear saturation density for  $\alpha = 0$ . Included are four phases: unpaired phase, BCS (BEC) phase, LOFF phase, and PS-BEC (PS-BEC) phase. For each asymmetry there are two tri-critical points, one of which is always a Lifshitz point [37]. For special values of asymmetry, these two points degenerate into a single tetra-critical point at  $\log(\rho/\rho_0) = -0.22$  and  $T = 2.85 \text{ MeV}$  when  $\alpha_4 = 0.255$  (shown by a square). The LOFF phase disappears at the point  $\log(\rho/\rho_0) = -0.65$  and  $T = 0$  (shown by a triangle) for  $\alpha = 0.62$ . The boundaries between BCS and BEC phases are identified by the change of sign of the average chemical potential  $\bar{\mu}$ . The diamonds (red online) mark the density and temperature values in the diagram that are used in the representative study (see Table I) of weak-coupling, intermediate-coupling, and strong-coupling regimes (from right to left).

and we assign the ground state to the phase with lowest free energy at any given temperature, density and isospin asymmetry. Inputs for the subsequent numerical calculations are the same as in paper I. Specifically, the pairing interaction is given by the bare nucleon-nucleon interaction in the  ${}^3S_1$ - ${}^3D_1$  partial wave, based on the (phase-shift equivalent) Paris potential [38]. The nuclear mean field is modeled by a Skyrme density functional, with SkIII [39] and SLy4 [40] parametrizations yielding nearly identical results. A computation of the effective mass from a realistic (e. g. Paris) potential would require a larger numerical effort within a beyond-mean-field microscopic many-body approach. However the effective masses computed from microscopic approaches agree well with those derived from Skyrme functionals and our results are not sensitive to small (of order of a few percent) variations in the effective mass.

### III. BCS PHASE, LOFF PHASE, AND CROSSOVER TO BEC

#### A. Phase diagram

The phase diagram of dilute nuclear matter is shown in Fig. 1 for several values of isospin asymmetry  $\alpha$ . Four different phases of matter are present [see Eq. (26)]. (a) The unpaired normal phase is always the ground state at sufficiently high temperatures  $T > T_{c0}$ , where  $T_{c0}(\rho)$  is the critical temperature of the normal/superfluid phase transition at  $\alpha = 0$ . (b) The LOFF phase is the ground state in a narrow temperature-density strip at low temperatures and high densities. (c) The domain of PS appears at low temperatures and low densities. Finally, (d) the isospin-asymmetrical BCS phase is the ground state at intermediate temperatures and intermediate to low densities. It is convenient at this point to define three regimes of coupling which are characterized solely by the density of the system, because the boundaries between these regimes are insensitive to the temperature. The strong-coupling regime (SCR) corresponds to the low-density limit where well-defined deuterons are formed, while the weak-coupling regime (WCR) corresponds to the high-density limit where well-defined Cooper pairs are present. In between these limiting cases we identify the intermediate-coupling regime (ICR). We delineate the boundaries between these regimes in the following discussion.

At the extreme of low density corresponding to the SCR, the BCS superfluid phases have two counterparts: The BCS phase evolves into the BEC phase of deuterons, whereas the PS-BCS phase evolves into the PS-BEC phase, in which the superfluid fraction of matter is a BEC of deuterons. The superfluid/unpaired phase transitions and the phase transitions between the superfluid phases are of second order (thin solid lines in Fig. 1), with the exception of the PS-BCS to LOFF transition, which is of first order (thick solid lines in Fig. 1). The BCS-BEC transition and the PS-BCS to PS-BEC transition are smooth crossovers. At nonzero isospin asymmetry, the phase diagram features two tri-critical points, i.e., points where the simpler pairwise phase coexistence terminates and three different phases coexist.

Consistent with the earlier studies of the BCS-BEC crossover, one observes in the phase diagram of Fig. 1 a smooth crossover to an asymptotic state corresponding to a mixture of a Bose condensate of deuterons and a gas of excess neutrons. This however occurs at moderate temperatures, where the unconventional phases do not appear. The new ingredient of the nuclear phase diagram is the crossover seen at very low temperatures, where the heterogeneous superfluid phase is replaced by a heterogeneous mixture of a phase containing a deuteron condensate and a phase containing neutron-rich unpaired nuclear matter.

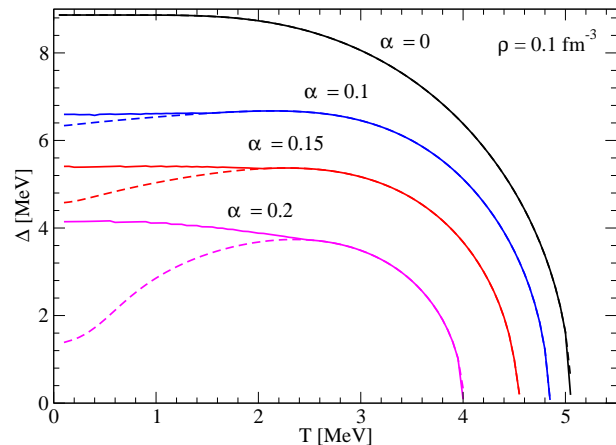


FIG. 2: (Color online) Gap as a function of temperature for asymmetry values  $\alpha = 0.0$  (black),  $\alpha = 0.1$  (blue),  $\alpha = 0.15$  (red) and  $\alpha = 0.2$  (magenta). Results allowing for the LOFF phase are traced by solid lines, those restricted to the BCS phase are traced by dashed lines.

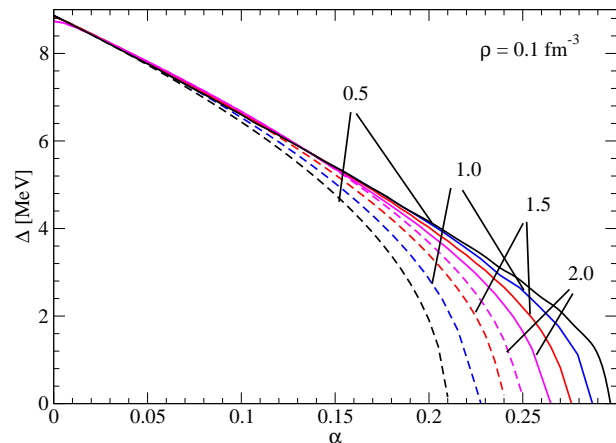


FIG. 3: (Color online) Gap as a function of asymmetry at constant density  $\rho = 0.1 \text{ fm}^{-3}$  for  $T = 0.5$  (black),  $T = 1.0$  MeV (blue),  $T = 1.5$  MeV (red),  $T = 2.0$  MeV (magenta). Results allowing for the LOFF phase are traced by solid lines; those restricted to the BCS phase are traced by dashed lines.

#### B. Temperature and asymmetry dependence of the gap: contrasting the BCS and LOFF phases

Before turning to the main topic of this work, we would like to recall and explore the behavior of the gap function as a function of temperature and asymmetry at constant density. We concentrate only on the WCR, as the behavior of the gap function in SCR is self-similar to that of the WCR. For now, we also neglect the possibility that the PS phase is the ground state. Figure 2 shows the weak-coupling gap as a function of temperature for a range of asymmetries. The plotted results for each nonzero value of  $\alpha$  reveal different regimes of rel-

atively low and relatively high temperature that reflect the different behaviors of the gap when the possibility of a LOFF phase is taken into account (solid curves) and when it is not (dashed curves). Two branches existing at lower temperatures merge at some point to form a single segment existing at higher temperatures. This high-temperature segment corresponds to the BCS state, and the temperature dependence of the gap is standard, with  $d\Delta(T)/dT < 0$  and asymptotic behavior  $\Delta(\alpha, T) \sim [T_c(\alpha)(T_c(\alpha) - T)]^{1/2}$  as  $T \rightarrow T_c(\alpha)$ , where  $T_c(\alpha)$  is the (upper) critical temperature. In the low-temperature region below the branch point, there are two competing phases (BCS and LOFF), with very different temperature dependences of the gap function. The quenching of the BCS gap (dashed lines) as the temperature is decreased is caused by the loss of coherence among the quasiparticles as the thermal smearing of the Fermi surfaces disappears. Consequently, in the low-temperature range below the branch point, the BCS branch shows the unorthodox behavior  $d\Delta(T)/dT > 0$ , and for large enough asymmetries there exists a lower critical temperature  $T_c^*$  [17]. On the contrary, one finds  $d\Delta(T)/dT < 0$  for the LOFF branch, as is the case in ordinary (symmetrical) BCS theory [41]. It should be mentioned that the ‘‘anomalous’’ behavior of the BCS gap below the point of bifurcation leading to the LOFF state gives rise to a number of anomalies in thermodynamic quantities, such as negative superfluid density or excess entropy of the superfluid [42]. These anomalies are absent in the LOFF state [43]. Figure 3 shows the dependence of the gap function on asymmetry for several pertinent temperatures. In accord with Fig. 2, there are two curves (or segments) for each temperature: one in the low- $\alpha$  domain where only the BCS phase exists and the other in the large- $\alpha$  domain where both BCS (dashed lines) and LOFF states (solid lines) are possible. Clearly the LOFF solution, for which the gap extends to larger  $\alpha$  values, is favored in the latter domain.

For small  $\alpha$  the gap function is linear in  $\alpha$ . At the other extreme of large  $\alpha$ , the gap has the asymptotic behavior  $\Delta(\alpha) \sim \Delta_{00} (1 - \alpha/\alpha_1)^{1/2}$ , where  $\alpha_1 \sim \Delta_{00}/\bar{\mu}$  and  $\Delta_{00}$  is the value of the gap at vanishing temperature and asymmetry. The critical asymmetry  $\alpha_2$  at which the LOFF phase transforms into the normal phase is a decreasing function of temperature, whereas that for termination of the BCS phase (denoted  $\alpha_1$  above) increases up to the temperature where  $\alpha_1 = \alpha_2$ . For larger temperatures,  $\alpha_1$  decreases with temperature. Consequently, in the dominant phase the critical asymmetry always decreases with temperature.

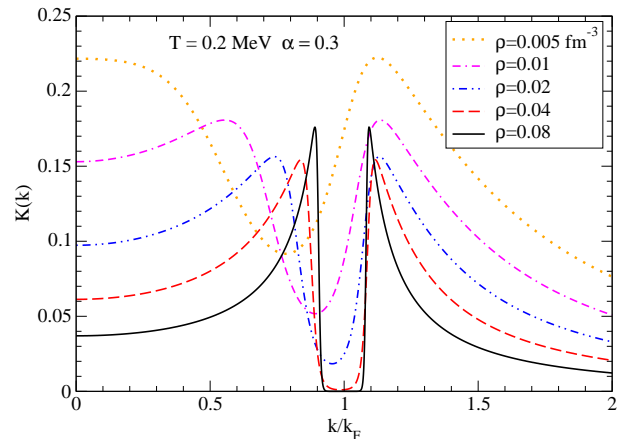


FIG. 4: (Color online) Dependence of the kernel  $K(k)$  on momentum in units of Fermi momentum for fixed  $T = 0.2$  MeV,  $\alpha = 0.3$ , and various densities indicated in the plot.

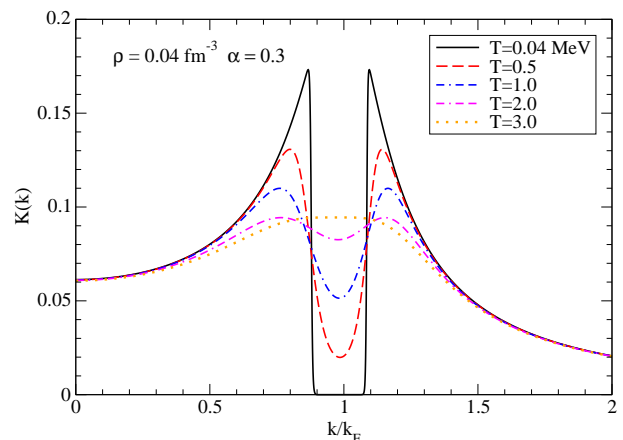


FIG. 5: (Color online) Dependence of the kernel  $K(k)$  on momentum in units of Fermi momentum for fixed  $\rho = 0.04$   $\text{fm}^{-3}$ ,  $\alpha = 0.3$ , and various temperature indicated in the plot.

### C. The kernel of the gap equations

The first intrinsic quantity chosen for detailed study is the kernel of the gap equation,

$$K(k, \theta) \equiv \sum_{a,r} \frac{P_r^a}{4\sqrt{E_S(k)^2 + \Delta^2(k, Q)}}. \quad (27)$$

This kernel is proportional to the imaginary part of the retarded anomalous propagator and the Pauli operator represented by  $P_r^a = 1 - 2f(E_r^a)$ . Physically,  $K(k)$  can be interpreted as the wave function of the Cooper pairs, because it obeys a Schrödinger-type eigenvalue equation in the limit of extremely strong coupling. Note that at Fermi surface  $E_S$  vanishes. The ranges of momenta which contribute substantially to the gap equation in different regimes of the phase diagram can be identified from

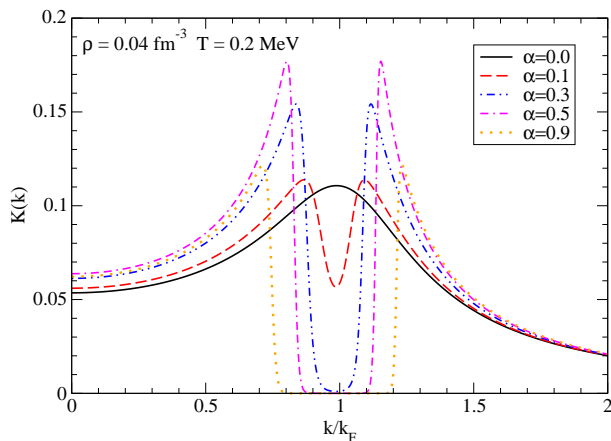


FIG. 6: (Color online) Dependence of the kernel  $K(k)$  on momentum in units of Fermi momentum for fixed  $\rho = 0.04 \text{ fm}^{-3}$ ,  $T = 0.2 \text{ MeV}$ , and various values of asymmetry indicated in the plot.

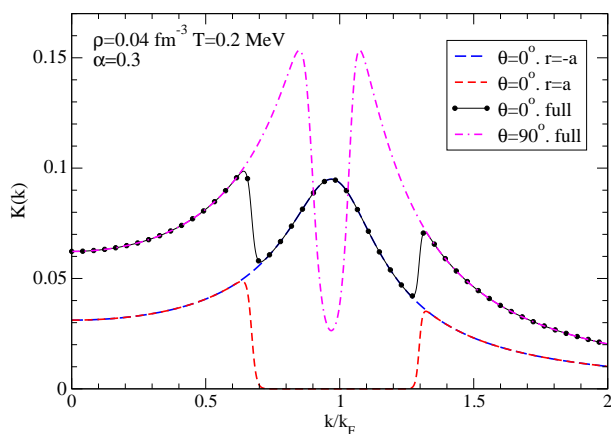


FIG. 7: (Color online) Dependence of the kernel  $K(k)$  on momentum in units of Fermi momentum at fixed  $\rho = 0.04 \text{ fm}^{-3}$ ,  $T = 0.2 \text{ MeV}$ , and  $\alpha = 0.3$  for the LOFF phase, where  $\theta$  is the angle formed by the c. m. and relative momenta in Eq. (27). In the case  $\theta = 0^\circ$  the full result (solid-filled-circle line) is decomposed into components with  $r = -a$  (long dashed line) and  $r = a$  (dash-dotted line).

Figs. 4-7. We now discuss the insights that can be gained from these figures in some detail.

Figure 4 shows the function  $K(k)$  at constant temperature and asymmetry for various densities. The high densities correspond to the BCS regime, and the low densities to the BEC regime, allowing us to follow the evolution of this function through the BCS-BEC crossover. In the BCS regime,  $K(k)$  has two sharp maxima which are separated by a depression of width  $\delta\mu$  around the Fermi momentum. Referring to the discussion of occupation numbers in Sec. III E below, this feature originates from the Pauli operator. Because of their strong localization in momentum space, the Cooper pairs have an

intrinsic structure that is broad in real space, implying a large coherence length. This is characteristic of the BCS regime. The picture is reversed in the strong-coupling (low-density) limit, where  $K(k)$  is a broad function of momentum, corresponding to the presence of bound states (deuterons), which are well-localized in real space. This is characteristic of the BEC regime. In addition, as the density decreases, the lower peak moves toward  $k = 0$ , owing to the fact that  $\bar{\mu}$  changes its sign from positive to negative at the transition from the BCS to the BEC regime. As a consequence, the prefactor of the Pauli operator  $P_a^r$  peaks at  $k = 0$  in the BEC regime, rather than at the Fermi surface as in the BCS regime.

Figure 5 shows the function  $K(k)$  for various temperatures, now at constant asymmetry and constant density, such that the system is situated in the BCS regime. At low temperatures,  $K(k)$  is seen to have two maxima separated by a depression around the Fermi momentum, as already discussed above. Increasing the temperature smears out the structures characteristic of the low-temperature case, owing to temperature-induced blurring of the Fermi surface. Close to  $T_c$ , the temperature effects dominate over the effects of asymmetry. Consequently, the double-peak structure disappears and the isospin asymmetry does not affect the properties of the condensate.

Figure 6 shows the function  $K(k)$  for various asymmetries at constant temperature and the same density as above (thus again implying the BCS regime). We can now follow how the double peak-structure builds up as the asymmetry is increased. Because the width of the depression is proportional to  $\delta\mu$ , it increases with increasing isospin asymmetry, a behavior consistent with the facts that the Fermi surfaces of neutrons and protons are pulled apart by the isospin asymmetry and that in the BCS regime the available phase space is constrained to the vicinity of the corresponding Fermi surface.

Finally, in Fig. 7 we show  $K(k)$  for fixed values of temperature, asymmetry, and density for the LOFF phase at two values of the angle formed by the relative and c. m. momenta, as defined in Eq. (27). It is seen from the figure that in the orthogonal case ( $\theta = 90^\circ$ ) the double-peak structure present in the BCS phase remains, although the effects of asymmetry are weaker compared to the BCS case. This is easily understood by noting that  $E_A = 0$  for  $\theta = 90^\circ$ , therefore finite momentum induces only a shift in the energy origin according to  $\bar{\mu} \rightarrow \bar{\mu} - Q^2/8m^*$ . The case  $\theta = 0^\circ$  exposes an interesting feature of the LOFF phase: For a range of orientations of the c. m. momentum of Cooper pairs ( $\theta \sim 0^\circ$ ), the effects of asymmetry are mitigated and the kernel obtains a maximum at  $k/k_F = 1$ , which is a combination of the contribution from  $r = -a$ , which acts to enhance the pairing correlations in the vicinity of the Fermi surface, and the  $r = a$  contribution which vanishes in this region.



### D. The Cooper-pair wave function across the BCS-BEC phase transition

The transition to the BEC regime of strongly coupled neutron-proton pairs, which are asymptotically identical with deuterons, occurs at low densities. The criterion for the transition from BCS to BEC is that either the average chemical potential  $\bar{\mu}$  changes its sign from positive to negative values, or the coherence length  $\xi$  of a Cooper pair becomes comparable to the interparticle distance, i.e.,  $\xi$  becomes of order  $d \sim \rho^{-1/3}$ . (In the BCS regime  $\xi \gg d$ , whereas in the BEC regime  $\xi \ll d$ .)

The coherence length can be related to the root mean square of the Cooper-pair wave function, as we show below. The wave function of a Cooper pair is defined in terms of the kernel of the gap equation according to

$$\Psi(\mathbf{r}) = \sqrt{N} \int \frac{d^3p}{(2\pi)^3} [K(\mathbf{p}, \Delta) - K(\mathbf{p}, 0)] e^{i\mathbf{p}\cdot\mathbf{r}}, \quad (28)$$

where  $N$  is a constant determined by the normalization condition

$$N \int d^3r |\Psi(\mathbf{r})|^2 = 1. \quad (29)$$

In Eq. (28) we subtract from the kernel its value  $K(\mathbf{p}, 0)$  in the normal state to regularize the integral, which is otherwise divergent. Cut-off regularization of this strongly oscillating integral is not appropriate. The mean-square radius of a Cooper pair is defined via the second moment of the probability density,

$$\langle r^2 \rangle = \int d^3r r^2 |\Psi(\mathbf{r})|^2. \quad (30)$$

The coherence length, i.e., the spatial extension of a Cooper pair, is then defined as

$$\xi_{\text{rms}} = \sqrt{\langle r^2 \rangle}. \quad (31)$$

Thus the change in the coherence length is related to the change of the condensate wave function across the BCS-BEC crossover. The regimes of strong and weak coupling can be identified by comparing the coherence length to the mean interparticle distance  $d = (3/4\pi\rho)^{1/3}$ . In the BCS regime the coherence length is given by the well-known analytical formula

$$\xi_a = \frac{\hbar^2 k_F}{\pi m^* \Delta}. \quad (32)$$

Table I lists the analytical and root-mean-square values of the coherence length for several densities and temperatures, chosen to represent the different regimes WCR, ICR, and SCR, together the corresponding values of the mean interparticle distance. It is seen that in the case of neutron-proton pairing, one of the criteria for the BCS-BEC transition is fulfilled, namely, the mean distance between the pairs becomes larger than the coherence length

	$\log_{10} \left( \frac{\rho}{\rho_0} \right)$	$k_F [\text{fm}^{-1}]$	$T [\text{MeV}]$	$d [\text{fm}]$	$\xi_{\text{rms}} [\text{fm}]$	$\xi_a [\text{fm}]$
WCR	-0.5	0.91	0.5	1.68	3.17	1.41
ICR	-1.5	0.42	0.5	3.61	0.94	1.25
SCR	-2.5	0.20	0.2	7.79	0.57	1.79

TABLE I: For each of the three regimes of coupling strength, corresponding values are presented for the density  $\rho$  (in units of nuclear saturation density  $\rho_0 = 0.16 \text{ fm}^{-3}$ ), Fermi momentum  $k_F$ , temperature  $T$ , interparticle distance  $d$ , and coherence parameters  $\xi_{\text{rms}}$  and  $\xi_a$ . The values of the gap and effective mass (in units of bare mass) at  $\alpha = 0$  in these three regimes are 9.39, 4.50, 1.44 MeV and 0.903, 0.989, 0.999, respectively. In the regime WCR, the LOFF phase is found in the vicinity of asymmetry  $\alpha = 0.49$ , for which  $\Delta = 1.27 \text{ MeV}$  and  $Q = 0.4 \text{ fm}^{-1}$ .

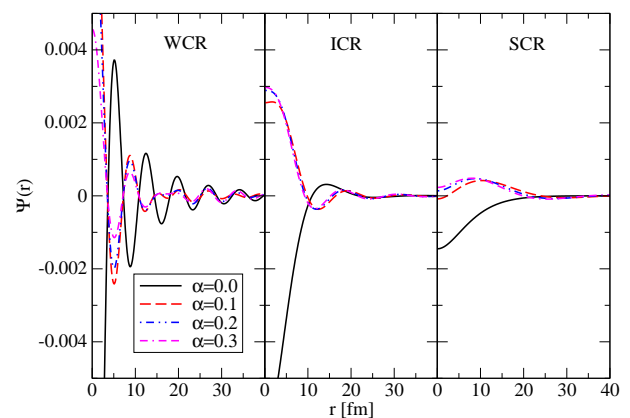


FIG. 8: (Color online) Dependence of  $\Psi(r)$  on  $r$  for the three coupling regimes and various values of asymmetry (see Table I for values of density and temperature).

of the superfluid as one goes from WCR to SCR. We have verified that the average chemical potential changes its sign accordingly, so that the second criterion is fulfilled as well. Figure 8 shows the wave function of Cooper pairs as a function of radial distance across the BCS-BEC crossover for various densities. In weak coupling, the wave function has a well-defined oscillatory form that extends over many periods of the interparticle distance. Such a state conforms to the familiar BCS picture, in which the spatial correlations are characterized by scales that are much larger than the interparticle distance. For intermediate and strong coupling the wave function is increasingly concentrated at the origin with at most a few periods of oscillation. The strong-coupling limit corresponds to pairs that are well localized in space within a small radius. This regime clearly has BEC character, with the pair correlations extending only over distances comparable to the interparticle distance. It is seen that in weak coupling the wave function is almost independent of the asymmetry, whereas in strong coupling this dependence is substantial. Figure 9, complementary to

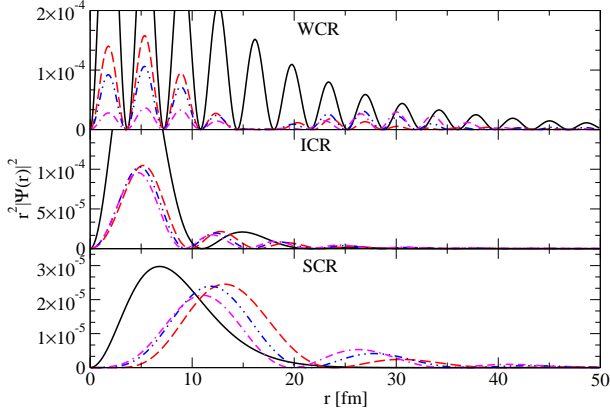


FIG. 9: (Color online) Dependence of  $r^2|\Psi(r)|^2$  on  $r$  for the three coupling regimes. Conventions are the same as in Fig. 8

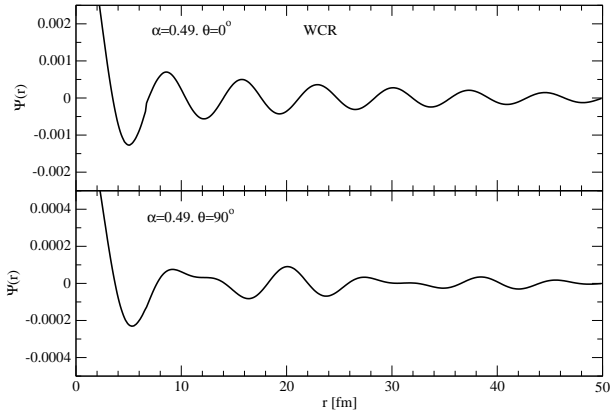


FIG. 10: Dependence of  $\Psi(r)$  on  $r$  in the regime WCR for two different angles  $\theta$  for asymmetry  $\alpha = 0.49$  at which the LOFF phase is the ground state.

Fig. 8, displays the quantity  $r^2|\Psi(\mathbf{r})|^2$ . The spatial correlation in the regime SCR is dominated by a single peak corresponding to a tightly bound state close to the origin. The existence of residual oscillations indicates that there is no unique bound state formed at such coupling, but the tendency towards its formation is clearly seen. An oscillatory structure appears in the ICR as a fingerprint of the transition from BEC to the BCS regime. In the WCR we observe oscillations over many periods, i.e., over large distances, indicative of the coherent BCS state. At low and high asymmetries the strong-coupling peaks are well defined, whereas at intermediate asymmetries the weight of the function is distributed among several peaks.

Figure 10 and 11 demonstrates the same quantities  $\Psi(\mathbf{r})$  and  $r^2|\Psi(\mathbf{r})|^2$  for the case of the LOFF phase computed at the WCR point of the phase diagram (as specified in Table I). At this point the LOFF phase is the ground state of the matter at asymmetry  $\alpha = 0.49$  ( $\delta\mu = 6.45$  MeV), where  $\Delta = 1.27$  MeV and  $Q = 0.4$

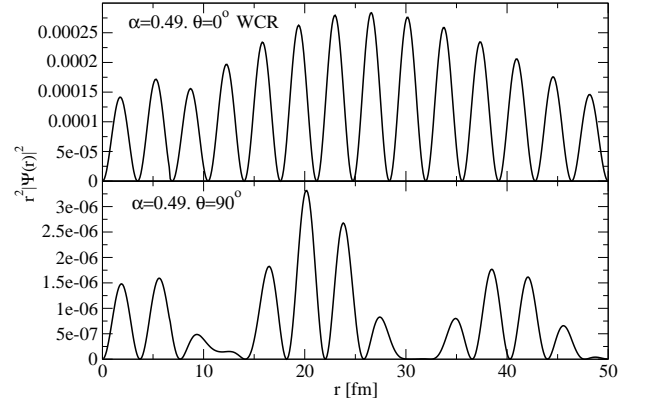


FIG. 11: Dependence of  $r^2|\Psi(r)|^2$  on  $r$  in the regime WCR for two different angles  $\theta$  for asymmetry  $\alpha = 0.49$  at which the LOFF phase is the ground state.

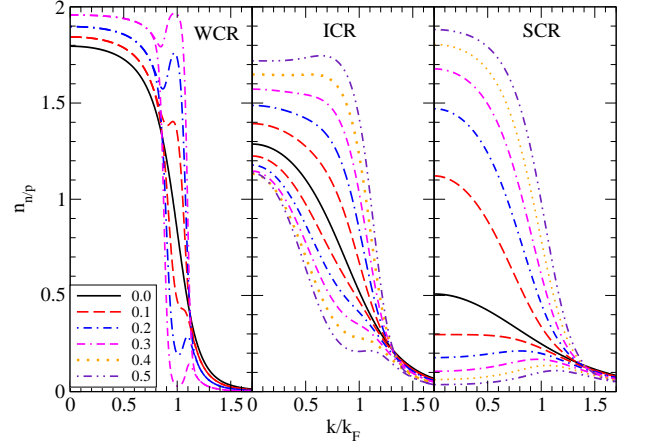


FIG. 12: (Color online) Dependence of the neutron and proton occupation numbers on momentum  $k$  (in units of Fermi momentum) for the three coupling regimes and various asymmetries indicated in the legend.

$\text{fm}^{-1}$ . For slightly lower asymmetries ( $\alpha \leq 0.48$ ) the system is in the PS phase, whereas for  $\alpha > 0.5$  the gap is vanishingly small, the system being in the normal state. In the case  $\theta = 0^\circ$  the perfect oscillatory behavior seen in  $\Psi(\mathbf{r})$  in the BCS case is replicated, as in this case the finite momentum of the condensate does not contribute to the spectrum of the Cooper pairs. In the case  $\theta = 90^\circ$   $\Psi(\mathbf{r})$  is distorted in the LOFF phase by the presence of a second oscillatory mode with the period  $2\pi/Q$  in addition to the first mode, with the period  $2\pi/k_F$ . The additional periodic structure is more pronounced in the quantity  $r^2|\Psi(\mathbf{r})|^2$ , where the rapid oscillations are modulated with a period  $\sim 16$  fm.

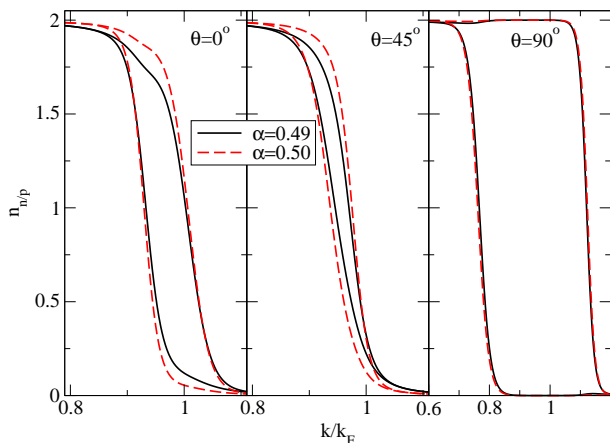


FIG. 13: (Color online) Dependence of the neutron and proton occupation numbers on momentum  $k$  (in units of Fermi momentum) in the WCR for two asymmetries where the LOFF phase is the ground state. The three angles indicated refer to the neutron occupation numbers. The proton occupation numbers are plotted for angles  $180^\circ - \theta$ .

### E. Occupation numbers

The integrand of Eq. (22) defines the occupation numbers  $n_{n/p}(k)$  of the neutrons and protons. These quantities are shown in different coupling regimes of the BCS-BEC crossover in Fig. 12. In the WCR (leftmost panel) the occupation numbers of protons exhibit a “breach” [44] or “blocking region” for large asymmetries, i.e., the minority component is entirely expelled from the blocking region ( $n_p = 0$ ), while the majority component is maximally occupied ( $n_n/2 = 1$ ). In the small- $\alpha$  limit the occupation numbers are clearly fermionic (with some diffuseness owing to the temperature) in that all single-particle states below a certain mode (the Fermi momentum at  $T = 0$ ) are almost filled, while all states above are nearly empty. We have verified that in the high-temperature limit the breach is filled in, the occupation numbers becoming smooth functions of momentum; consequently the low-momentum modes are less populated.

In the ICR (middle panel) the fermionic nature of the occupation numbers is lost. The low-momentum modes are not fully populated and, accordingly, high-momentum modes are more heavily occupied. A Fermi surface cannot be identified because of the smooth population of the modes. Moreover, a breach no longer appears for the parameters chosen. It is also to be noted that for large asymmetries  $\alpha \geq 0.4$ , the momentum dependence of the occupation numbers becomes non-monotonic; for the minority component this is a precursor of the change in the topology of the Fermi surface under increase of coupling strength.

The SCR (rightmost panel) can be identified with the BEC phase of strongly coupled pairs. At large asymmetries the distribution of the minority component under-

goes a topological change. First there develops an empty strip within the distribution function, which is reorganized at larger asymmetries into a distribution in which the modes are populated starting from a certain nonzero value. Thus, the Fermi sphere occupied by the minority component in the weakly coupled BCS limit evolves into a shallow shell structure in the strongly coupled Bose-Einstein-condensed limit. This behavior was already revealed in the case of the  ${}^3S_1$ - ${}^3D_1$  condensate in Ref. [18].

Figure 13 depicts the occupation numbers in the WCR at asymmetries corresponding to a LOFF-phase ground state for three fixed angles  $\theta = 0^\circ$ ,  $45^\circ$ , and  $90^\circ$ . In the case  $\theta = 90^\circ$  we have  $E_A = 0$ , and the LOFF spectrum differs from the asymmetrical BCS spectrum only by a shift in the energy origin,  $\bar{\mu} \rightarrow \bar{\mu} - Q^2/8m^*$ . Therefore the occupation numbers do not depart qualitatively from their BCS behavior; moreover, the “breach” is clearly seen. For  $\theta = 45^\circ$  the difference between the occupation numbers disappears, i.e., the superconductor behaves as if it were isospin symmetric. This result follows from the fact that the nonzero c. m. momentum of the LOFF phase compensates for the mismatch of the Fermi spheres and restores the coherence needed for pairing. In the case  $\theta = 0^\circ$  the effect of  $E_A$  attains its maximal value, but the occupation numbers are intermediate between those of the two cases previously addressed. This is attributable to the fact that the overlap between the spectra of neutron and proton quasiparticle branches is better for  $\theta = 45^\circ$  than for  $\theta = 0^\circ$ , in which case the quasiparticle spectra “overshoot” the optimal overlap (see the discussion in the following section).

### F. Quasiparticle spectra

Finally, let us consider the dispersion relations for quasiparticle excitations about the  ${}^3S_1$ - ${}^3D_1$  condensate. We first examine in some detail the spectra  $E_{\pm}^a$  in the BCS case defined in Eq. (19), which are then independent of the sign of  $a$  and we take  $a = +$ . These are shown in Fig. 14 for the three coupling regimes of interest. In the isospin-symmetric BCS case, the dispersion relation has a minimum at  $E_{\pm}^+ = E_{\pm}^- = \Delta$  for  $k = k_F$ . For finite asymmetries one has  $E_{\pm}^{\pm} = \sqrt{E_S^2 + \Delta^2} \pm \delta\mu$ ; hence the minima of the dispersion relations of neutron and proton quasiparticles are given by an asymmetry-dependent gap value modified by the shift in chemical potential, i.e.,  $\Delta(\alpha) \pm \delta\mu$ . For protons this leads to a gapless spectrum, which does not require a finite minimum energy for excitation of two modes (say  $k_1$  and  $k_2$ ) for which the dispersion relation intersects the zero-energy axis. This phenomenon is well known as *gapless superconductivity*. The momentum interval  $k_1 \leq k \leq k_2$  corresponds to the interval in Fig. 12 where the occupation numbers of majority and minority components separate and the “breach” in the occupation of the minority component becomes prominent.

Consider now the SCR, in which case we are deal-

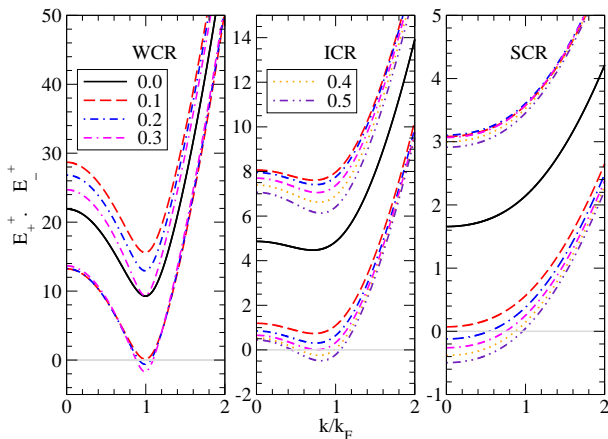


FIG. 14: (Color online) Dispersion relations for quasiparticle spectra in the case of the BCS condensate, as functions of momentum in units of Fermi momentum. For each asymmetry, the upper branch corresponds to  $E_+$ , and the lower to the  $E_-$  solution.

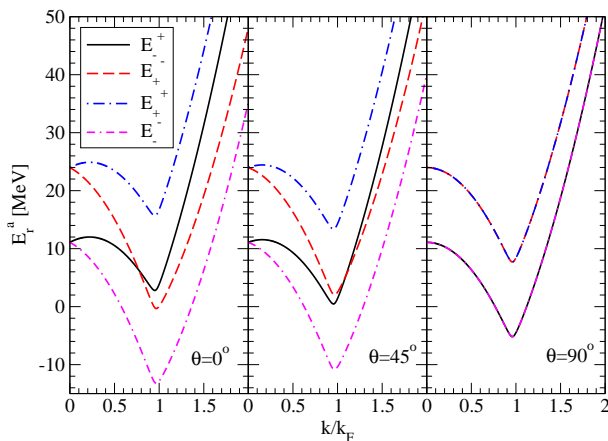


FIG. 15: (Color online) Dispersion relations for quasiparticle spectra in the LOFF phase for three angles and  $\alpha = 0.49$ .

ing with a gas of deuterons and free neutrons. In the symmetrical limit (i.e. when only deuterons are present), the dispersion relation has a minimum at the origin that corresponds to the (average) chemical potential, which asymptotically approaches half the binding energy of a deuteron in vacuum [18]. The effect of asymmetry is to shift the average chemical potential downwards and to introduce the separation  $\delta\mu$  in the quasiparticle spectra.

Because the minimum is now at the origin, there is only one mode for which the dispersion relation crosses zero at a finite  $k$ . The dispersion relations in the ICR experience a transition from the WCR to the SCR, such that their key features resemble those of the WCR, but with a shallower minimum and a larger momentum interval  $[k_1, k_2]$  over which the excitation spectrum becomes gapless.

The dispersion relations for quasiparticles in the LOFF phase for special angles  $\theta$  are shown in Fig. 15 in the WCR and for  $\alpha$  values corresponding to the LOFF phase as ground state. In this case, we show all four branches of quasiparticle spectrum. Consistent with the earlier discussion of Fig. 13 for  $\theta = 90^\circ$ , the LOFF phase resembles the BCS phase and there is a large mismatch between the spectra of protons and neutrons. In this case the branches  $a = +$  and  $a = -$  are degenerate. For other angles we see again that the nonzero c. m. momentum mitigates the asymmetry and brings the quasiparticle spectra closer together, i.e., the LOFF phase resembles the symmetrical BCS phase for the two branches with  $a \neq r$  for  $\theta < 90^\circ$ . This is particularly clear for  $\theta = 45^\circ$ , in which case two of the four dispersion relations coincide in the vicinity of the Fermi momentum. It is clear that the optimal mitigation of the isospin mismatch by the finite moment does not need to be for  $\theta = 0^\circ$ , but can occur at some angle  $0^\circ \leq \theta \leq 90^\circ$ ; it is seen that for  $\theta = 0^\circ$  the branches cross and, hence, “overshoot” the optimal compensation.

The restoration of the coherence (Fermi-surface overlap) in the LOFF phase can be illustrated by looking at the solutions of  $\epsilon_{n/p, \uparrow/\downarrow}^\pm = 0$  [see Eq. (8)] which define the Fermi-surface in the limit  $\Delta \rightarrow 0$  but  $Q \neq 0$ . These are illustrated in Fig. 16 in two cases,  $Q = 0$  and  $Q \neq 0$ . In the first case the Fermi surfaces are concentric spheres which have no intersection. In the second case the non-zero c. m. leads to an intersection of the Fermi-spheres; in these regions of intersection the pair correlations are restored to the magnitude characteristic to the BCS phase. Of course, the c. m. momentum costs positive kinetic energy, which must be smaller than the negative condensation energy for LOFF phase to be stable.

#### IV. CONCLUSION

Low-density nuclear matter is predicted to feature a rich phase diagram at low temperatures and nonzero isospin asymmetry. The phase diagram contains at least the following phases: the translationally and rotationally symmetric, but isospin-asymmetrical BCS phase, the BEC phase containing neutron-proton dimers, the current-carrying LOFF phase, and associated phase-separated phases.

Our analysis of these phases can be summarized as follows.

- The phase diagram of nuclear matter composed of these phases has two tri-critical points in general, one of which is a Lifshitz point. These can combine in a tetra-critical point for a special combination of density, temperature, and isospin asymmetry. The phase diagram contains two types of crossovers from the asymmetrical BCS phase to the BEC of deuterons and an embedded neutron gas: a transition between the homogeneous BCS-BEC phases at

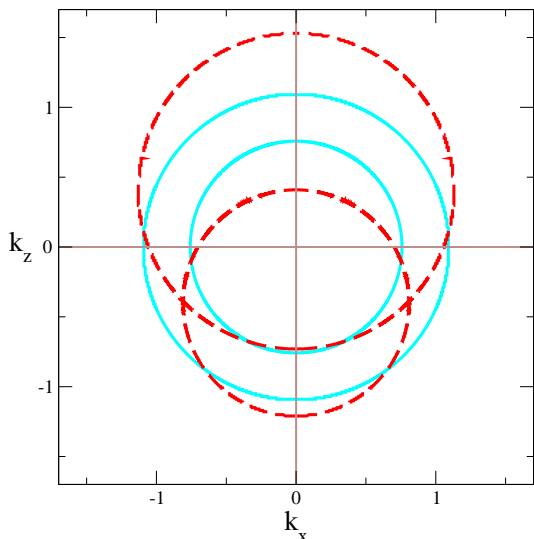


FIG. 16: (Color online) Illustration of Fermi surfaces in the asymmetrical BCS state (solid lines) and LOFF phase (dashed lines). The LOFF phase is characterized by the following values of parameters:  $\alpha = 0.49$ ,  $\delta\mu = 6.45$  MeV,  $\Delta = 1.27$  MeV and  $Q = 0.4$  fm $^{-1}$ .

relatively high temperatures and between the heterogeneous BCS-BEC phases at low temperatures. We have shown that the LOFF phase exists only in a narrow strip in the high-density, low-temperature domain and at nonzero asymmetries.

- The crossovers of BCS-BEC type are smooth and are characterized by lines in the temperature-density plane that are insensitive to the isospin asymmetry. These lines were obtained by examining the sign of the average chemical potential.
- Detailed analysis of key intrinsic quantities, including the kernel of the gap equation along with the Cooper-pair wave function and its probability density, clearly establishes that in the BCS limit one deals with a coherent state, whose wave function oscillates over many periods with a wavelength characterized by the inverse Fermi momentum  $k_F^{-1}$ . In the opposite limit the wave function is well-localized around the origin, indicating that one is then dealing with a Bose condensate of strongly bound states, namely deuterons.
- The analysis of the kernel of the wave function, the occupation probabilities of neutrons and protons, and the quasiparticle dispersion relations demonstrates the prominent role played by the Pauli-blocking region (called “the breach”) [44] that appears in these quantities. In the BCS phase and the low-temperature limit of the WCR, the blocking region embraces modes in the range  $k_1 \leq k \leq k_2$

around the Fermi surface. In this modal region, it has been found that (a) the minor constituents (protons) are extinct; (b) there are no contributions to the kernel of the gap equation from these modes; and (c) the end of points of this region correspond to the onset of gapless modes that can be excited without any energy cost. The LOFF phase appearing in this regime substantially mitigates the blocking mechanism by allowing for nonzero c. m. momentum of the condensate. As a consequence, all the intrinsic quantities studied are much closer to those of the isospin-symmetric BCS state.

- We have traced the evolution of the targeted intrinsic properties into the SCR as the system crosses over from the BCS condensate to a BEC of deuterons plus a neutron gas. In the SCR the long-range coherence of the condensate is lost. The dispersion relations change their form from a spectrum having a minimum at the Fermi surface to a spectrum that is minimal at  $k = 0$ , as would be expected for a BEC, independent of isospin asymmetry. With increasing isospin asymmetry, the proton dispersion relation acquires points with zero excitation energy in this regime. The occupation numbers reach a maximum for finite  $k$  and reflect a change of topology at large asymmetries: The filled “Fermi sphere” becomes an empty “core.”

The present investigation of BCS-BEC crossovers with inclusion of unconventional phases, such as the LOFF phase and the heterogeneous phase-separated phase, could be useful in the studies of spin/flavor-imbalanced fermionic systems in ultracold atomic gases, for recent studies see, e.g., Refs. [45–47], dense quark matter (e.g., Refs. [48–52]), and other related quantum systems.

### Acknowledgments

M. S. acknowledges the support by the HGS-HIRe graduate program at Frankfurt University. A. S. is supported by the Deutsche Forschungsgemeinschaft (Grant No. SE 1836/3-1) and thanks the Institute for Nuclear Theory at the University of Washington, Seattle, for its hospitality, and the Department of Energy for partial support during the program “Binary Neutron Star Coalescence as a Fundamental Physics Laboratory.” X. G. H. is supported by Fudan University Grant No. EZH1512519 and Shanghai Natural Science Foundation Grant No. 14ZR1403000. J. W. C. acknowledges research support from the McDonnell Center for the Space Sciences and expresses his thanks to Professor José Luís da Silva and his colleagues at Centro de Ciências Matemáticas for gracious hospitality at the University of Madeira.

- 
- [1] P. Nozières and S. Schmitt-Rink, *Journal of Low Temperature Physics* **59**, 195 (1985).
- [2] D. M. Eagles, *Physical Review* **186**, 456 (1969).
- [3] T. Alm, B. L. Friman, G. Röpke, and H. Schulz, *Nuclear Physics A* **551**, 45 (1993).
- [4] M. Baldo, U. Lombardo, and P. Schuck, *Phys. Rev. C* **52**, 975 (1995).
- [5] H. Stein, A. Schnell, T. Alm, and G. Röpke, *Zeitschrift für Physik A Hadrons and Nuclei* **351**, 295 (1995).
- [6] U. Lombardo and P. Schuck, *Phys. Rev. C* **63**, 038201 (2001).
- [7] A. Sedrakian and J. W. Clark, *Phys. Rev. C* **73**, 035803 (2006).
- [8] S. Mao, X. Huang, and P. Zhuang, *Phys. Rev. C* **79**, 034304 (2009).
- [9] X.-G. Huang, *Phys. Rev. C* **81**, 034007 (2010).
- [10] M. Jin, M. Urban, and P. Schuck, *Phys. Rev. C* **82**, 024911 (2010).
- [11] A. Sedrakian, *Journal of Physics Conference Series* **413**, 012024 (2013).
- [12] M. Stein, A. Sedrakian, X.-G. Huang, J. W. Clark, and G. Röpke, *Journal of Physics Conference Series* **496**, 012008 (2014).
- [13] A. Pastore, J. Margueron, P. Schuck, and X. Viñas, *Phys. Rev. C* **88**, 034314 (2013).
- [14] X.-I. Shang and W. Zuo, *Phys. Rev. C* **88**, 025806 (2013).
- [15] X. Shang and W. Zuo, *ArXiv e-prints: 1308.0364* (2013).
- [16] B. Y. Sun and W. Pan, *Nuclear Physics A* **909**, 8 (2013).
- [17] A. Sedrakian and U. Lombardo, *Physical Review Letters* **84**, 602 (2000).
- [18] U. Lombardo, P. Nozières, P. Schuck, H.-J. Schulze, and A. Sedrakian, *Phys. Rev. C* **64**, 064314 (2001).
- [19] B. Cederwall, F. G. Moradi, T. Bäck, A. Johnson, J. Blomqvist, E. Clément, G. de France, R. Wadsworth, K. Andgren, K. Lagergren, et al., *Nature (London)* **469**, 68 (2011).
- [20] S. Typel, G. Röpke, T. Klähn, D. Blaschke, and H. H. Wolter, *Phys. Rev. C* **81**, 015803 (2010).
- [21] S. Heckel, P. P. Schneider, and A. Sedrakian, *Phys. Rev. C* **80**, 015805 (2009).
- [22] A. Sedrakian, *Phys. Rev. C* **63**, 025801 (2001).
- [23] H. Müther and A. Sedrakian, *Phys. Rev. C* **67**, 015802 (2003).
- [24] A. I. Larkin and Y. N. Ovchinnikov, *Zh. Eksp. Teor. Fiz.* **47**, 762 (1965).
- [25] P. Fulde and R. A. Ferrell, *Physical Review* **135**, 550 (1964).
- [26] P. F. Bedaque, H. Caldas, and G. Rupak, *Physical Review Letters* **91**, 247002 (2003).
- [27] H. Müther and A. Sedrakian, *Physical Review Letters* **88**, 252503 (2002).
- [28] M. Matsuo, *Phys. Rev. C* **73**, 044309 (2006).
- [29] J. Margueron, H. Sagawa, and K. Hagino, *Phys. Rev. C* **76**, 064316 (2007).
- [30] A. A. Isayev, *Phys. Rev. C* **78**, 014306 (2008).
- [31] Y. Kanada-En'yo, N. Hinohara, T. Suhara, and P. Schuck, *Phys. Rev. C* **79**, 054305 (2009).
- [32] T. Abe and R. Seki, *Phys. Rev. C* **79**, 054002 (2009).
- [33] B. Y. Sun, H. Toki, and J. Meng, *Physics Letters B* **683**, 134 (2010).
- [34] L. Salasnich, *Phys. Rev. C* **84**, 067301 (2011).
- [35] T. T. Sun, B. Y. Sun, and J. Meng, *Phys. Rev. C* **86**, 014305 (2012).
- [36] M. Stein, X.-G. Huang, A. Sedrakian, and J. W. Clark, *Phys. Rev. C* **86**, 062801 (2012).
- [37] R. M. Hornreich, *Journal of Magnetism and Magnetic Materials* **15**, 387 (1980).
- [38] J. Haidenbauer and W. Plessas, *Phys. Rev. C* **30**, 1822 (1984).
- [39] R. K. Su, S. D. Yang, and T. T. S. Kuo, *Phys. Rev. C* **35**, 1539 (1987).
- [40] E. Chabanat, P. Bonche, P. Haensel, J. Meyer, and R. Schaeffer, *Nuclear Physics A* **635**, 231 (1998).
- [41] L. He, M. Jin, and P. Zhuang, *Phys. Rev. B* **74**, 214516 (2006).
- [42] A. Sedrakian, H. Müther, and A. Polls, *Physical Review Letters* **97**, 140404 (2006).
- [43] M. Jin, L. He, and P. Zhuang, *International Journal of Modern Physics E* **16**, 2363 (2007).
- [44] E. Gubankova, W. V. Liu, and F. Wilczek, *Physical Review Letters* **91**, 032001 (2003).
- [45] D. E. Sheehy and L. Radzihovsky, *Annals of Physics* **322**, 1790 (2007).
- [46] S. Giorgini, L. P. Pitaevskii, and S. Stringari, *Reviews of Modern Physics* **80**, 1215 (2008).
- [47] A. Sedrakian, *Journal of Physics Conference Series* **321**, 012028 (2011).
- [48] A. Sedrakian and D. H. Rischke, *Phys. Rev. D* **80**, 074022 (2009).
- [49] C.-F. Mu, L.-Y. He, and Y.-X. Liu, *Phys. Rev. D* **82**, 056006 (2010).
- [50] J. Moreira, B. Hiller, W. Broniowski, A. A. Osipov, and A. H. Blin, *Phys. Rev. D* **89**, 036009 (2014).
- [51] I. E. Frolov, V. C. Zhukovsky, and K. G. Klimenko, *Phys. Rev. D* **82**, 076002 (2010).
- [52] T. Kojo, Y. Hidaka, K. Fukushima, L. D. McLerran, and R. D. Pisarski (2012). *Nucl. Phys. A* **875**, 94 (2012).